

PACS numbers: 52.38.Ph; 07.85.Fv
DOI: 10.1070/QE2002v032n02ABEH002148

Debris-free pulsed xenon-jet soft X-ray radiation source driven by Nd-laser radiation

V.G.Kapralov, R.Korde, V.E.Levashov, A.S.Pirozhkov, E.N.Ragozin

***Abstract*. A 'clean' (debris-free) pulsed soft X-ray radiation source was realised. The source is excited by the nanosecond pulses of a solid-state laser in a pulsed xenon gas jet (gas cloud). The source images are obtained at a wavelength of 180 Å using a focusing X-ray multilayer mirror. The spectra of the source are recorded in the 125 – 250 Å range using a stigmatic spectrograph comprising a recently developed broadband aperiodic multilayer mirror and a large-aperture transmission diffraction grating. The yield of soft X-rays was determined employing a fast-response absolutely calibrated AXUV-5 X-ray photodiode.**

Keywords: *laser plasma, gas-puff target, xenon, soft X-ray radiation, absolutely calibrated photodiode, stigmatic spectrograph, multilayer mirrors.*

1. Introduction

In recent years, a pulsed gas jet (a gas cloud) produced with a pulsed high-pressure gas nozzle was employed as a target in many laser-plasma experiments. The gas puff occupies a small volume in a laser target of this type, which favours the input of high-power heating laser radiation and the extraction of soft X-ray radiation (SXR). Another advantage of this approach is the possibility of producing a uniform active medium with low electron density gradients to minimise SXR refraction. Many papers have been devoted to the study of the resulting plasma as an SXR laser active medium. In many of these papers, the collisional scheme for producing inversion on transitions of multiply charged ions was used. Gain on the transitions of Ne-like Ar ($\lambda = 469$ Å) and Ni-like Xe ($\lambda = 100$ Å) was demonstrated in an elongated (up to 3 cm) gas target driven by subnanosecond laser pulses with an energy up to 600 J [1]. The effect of a small admixture of high-Z elements (Ar, Kr, Xe) on the radiative cooling rate of a laser-produced nitrogen plasma was investigated with the aim of developing a recombination SXR laser [2]. A gas cloud can serve as a nonlinear medium for the generation of high-order laser-radiation harmonics whose spectrum extends to the SXR range down to ~ 100 Å and below [3]. Recently, the authors of paper [4] reported the generation of a train of ~ 250-as SXR pulses by focusing femtosecond laser pulses into an argon jet. The plasma of a pulsed xenon target excited by a nanosecond laser is also considered as a possible source of spontaneous SXR for projection X-ray lithography [5].

In this paper, we investigate the spectral, spatial and brightness characteristics of a compact laboratory SXR source driven by solid-state laser pulses, which are focused into a pulsed jet (cloud) of an inert gas (Xe) in vacuum. A source of this kind can be used, in particular, in absorption spectroscopy, reflectometry, X-ray optics research, etc. An advantage of a pulsed gas target is that the surface of optical components (both in the visible and X-ray ranges) and of radiation detectors is almost not contaminated. The contamination of optics by target fragments inevitably occurs when a solid laser target is used, which has rather long been employed in reflectometry [6] and X-ray optics research [7, 8].

2. Experimental facility

We performed experiments in a vacuum 3.8-m long chamber 0.9 m in diameter, in which an optical table of size 0.6×3.6 m for mounting optical components was placed (Fig. 1). This provided freedom in choosing opto-spectral schemes for X-ray diagnostics. A solid-state laser was located on the optical table adjacent to the end flange of the vacuum chamber. The laser beam was injected through a window in the flange. The chamber was evacuated to a pressure of 10^{-4} Torr employing a turbomolecular pump with a capacity of 2500 L s^{-1}. Three side ports each 0.75 m in diameter provided access to the chamber volume.

The gas jet (cloud) in vacuum was produced with a pulsed high-pressure electromagnetic valve timed with a laser shot. The gas (Xe in this case) issued into vacuum through a nozzle in the form of a 1-cm long channel 0.4 mm in diameter. When the valve was put to a test with an argon filling, 0.33 cm^3 of the gas was injected into vacuum on actuation. With xenon, the volume of gas exhausted is nearly two times smaller. On actuation of the valve filled with xenon at a pressure of 7 – 10 bar, we observed a short-term pressure rise up to $(3-4)\times10^{-4}$ Torr. In our experiments, the peak gas pressure above the nozzle was 10 bar.

V.G.Kapralov St. Petersburg State Technical University, Politekhnicheskaya ul. 29, 195251 St. Petersburg, Russia;
R.Korde International Radiation Detectors, Inc., 2527 West 237th Street, Unit B, Torrance, CA 90505-5243, USA;
V.E.Levashov, A.S.Pirozhkov, E.N.Ragozin P.N.Lebedev Physics Institute, Russian Academy of Sciences, Leninsky prosp., 53, 119991 Moscow, Russia; e-mail: ragozin@sci.lebedev.ru

Received 27 November 2001
Kvantovaya Elektronika **32** (2) 149 – 154 (2002)
Translated by E.N.Ragozin

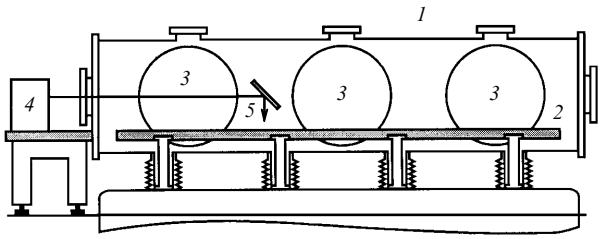

Figure 1. Schematic diagram of the basic parts of the experimental facility (side view):
(*1*) vacuum chamber 0.9 m in diameter and 3.8 m in length; (*2*) optical table measuring 0.6 by 3.6 m for mounting optical components; (*3*) side ports 0.75 m in diameter, which provide access to the chamber interior; (*4*) solid-state laser on an optical table attached to the end flange of the vacuum chamber; (*5*) laser beam.

The gas jet was irradiated by pulses from a Nd:$YAlO_3$ solid-state laser ($\lambda = 1.08$ μm, $Q = 0.4$ J, $\tau_p = 6$ ns). The beam divergence was estimated at 2.5×10^{-4} rad (50 % of the energy). The laser was made on the generator–amplifiers principle and contained a passively Q-switched single-mode master oscillator with an active element 6 mm in diameter and two amplifiers with active elements 8 and 12 mm in diameter. To suppress amplified luminescence and prevent self-excitation, we used a Faraday isolator based on a TGG crystal in the field of a permanent magnet and also a saturable absorber with a long service life. The synchronising pulse fed to the laser power unit was delayed by a period of 0.3–1.3 ms relative to the instant of valve actuation; in this case, the laser pulse was delayed by 0.8–1.8 ms. A lens with a focal length $f = 63$ mm focused the laser beam into the xenon jet at a distance of ~ 0.5 mm from the exit nozzle orifice. Because of the radiation losses accompanying the injection of the beam into the chamber and its focusing, the energy of the laser beam at the target was 0.35 J. The jet axis was horizontal and the laser beam was directed downwards (Fig. 2).

Experiments involved recording the spectra of the resultant plasma in the 125–250 Å range, its images in the radiation with wavelengths $\lambda \approx 175 - 185$ Å, and also the absolute emission intensity in the latter wavelength interval centred at $\lambda = 180$ Å. In addition, a VChD-2 calorimeter was placed in the beam path below the nozzle to measure the fraction of laser energy transmitted through the gas jet (Fig. 2).

The plasma spectrum was recorded with a recently developed broadband stigmatic spectrograph [9], which comprised a focusing aperiodic normal-incidence multilayer mirror (Mo/Si, diameter $D = 50$ mm, radius of curvature $R = 1$ m) and a large-aperture free-standing transmission diffraction grating (1000 or 5000 lines mm^{-1}) (Fig. 3). The aperiodic multilayer mirror possessed a nearly uniform reflection in the 125–250 Å range and defined the operating spectral range of the spectrograph. (The potentialities of aperiodic multilayer structures were discussed in Refs [10–12].) The short-wavelength bound of the operating wavelength range was defined by the L absorption edge of silicon, below which the reflectivity of Mo/Si multilayers declines steeply. The reciprocal linear dispersion of the schemes with both gratings could be adjusted by varying the grating–film distance and was equal to 20 and 5 Å mm^{-1} in this series of measurements. The spectrum was recorded on UF-4 X-ray photographic film.

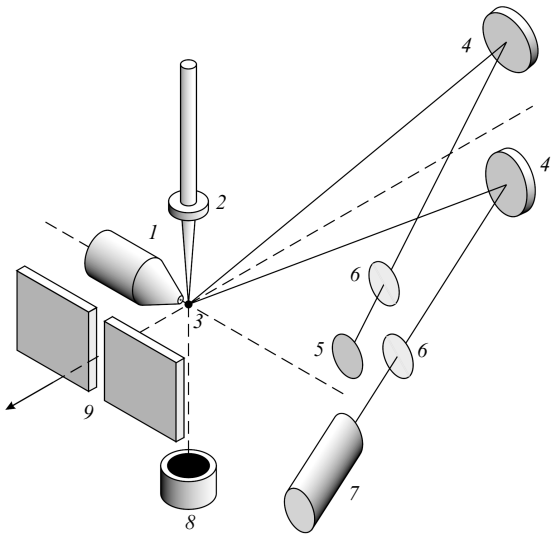

Figure 2. Arrangement of diagnostic instrumentation in experiments with a pulsed gas target:
(*1*) high-pressure pulsed gas valve; (*2*) lens for focusing the laser beam; (*3*) xenon plasma at the lens focus; (*4*) similar periodic multilayer mirrors (reflectivity peaks at $\lambda_0 = 180$ Å, half-height width of the reflection peak $\Delta\lambda_{1/2} = 10$ Å); (*5*) film holder with a UF-4 photographic film; (*6*) large-aperture free-standing aluminium filters; (*7*) AXUV-5 photodiode; (*8*) VChD-2 calorimeter; (*9*) entrance slit of the diffraction grating spectrograph.

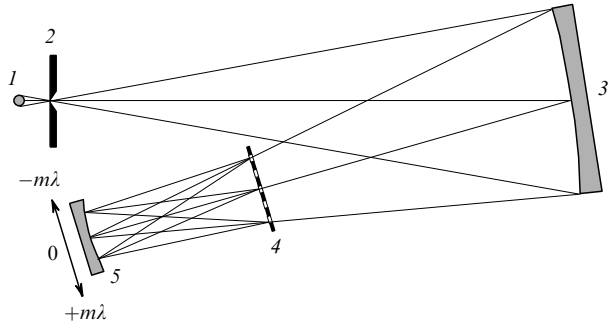

Figure 3. Schematic layout of the high-throughput stigmatic spectrograph:
(*1*) plasma; (*2*) entrance slit; (*3*) focusing aperiodic multilayer mirror ($D = 50$ mm, $R = 1$ m); (*4*) large-aperture transmission diffraction grating (1000 or 5000 lines mm^{-1}); (*5*) film holder with an X-ray photographic film.

The X-ray plasma images were obtained employing a focusing periodic multilayer mirror ($D = 60$ mm, $R = 2$ m) with a reflectivity peak at $\lambda_0 = 180$ Å and the full width at half-maximum of the resonance reflection peak $\Delta\lambda_{1/2} =$ 10 Å. The images were recorded on UF-4 X-ray photographic film. A similar focusing multilayer mirror ($\lambda_0 =$ 180 Å) transferred the X-ray image of the source to the sensitive surface of a fast-response absolute-calibrated AXUV-5 photodiode, which possesses a sensitivity of about 0.2 A W^{-1} in the spectral range of interest. The diameter of the photosensitive photodiode area was 2.5 mm, which significantly exceeded the source dimension (see below). In both channels, large-aperture thin-film 0.2 μm aluminium filters on a support mesh were placed in the beam path,

which served the function of rejecting the visible and near-UV radiation. The pulsed signal from the photodiode was fed to the amplifier input of a dual-beam S8-14 storage oscilloscope using a coaxial cable via a hermetic radio-frequency connector located in one of small auxiliary flanges of the vacuum chamber. A negative bias up to – 100 V was applied to the photodiode.

3. Results of measurements

Time-integrated X-ray source images were recorded with a focusing multilayer mirror with a small magnification ($1.27^{\times}$). Fig. 4 shows a source photograph obtained in one laser shot. Two emission peaks are observed: the upper one, occurring in the peripheral region of the xenon jet, and the lower one, shifted slightly upwards relative to the nozzle axis. In addition to the X-ray xenon plasma image, also present in the photograph is the nozzle shadow, which was obtained with the same multilayer mirror by backlighting the nozzle with visible light upon removing the aluminium filter. The presence of the shadow nozzle image gives a clear idea of the mutual arrangement of the X-ray source and the nozzle. One can see that the laser beam axis passes at a distance of 0.5 mm from the nozzle, where the atomic gas density on the jet axis is estimated at $\sim 1\%$ of the initial density, i.e., $\sim 2 \times 10^{18}$ cm^{-3} for an initial gas pressure of 8 bar.

The source dimension in the horizontal x-direction is 0.2 mm (the effective width) and ~ 0.4 mm by the base. In all photographs, the X-ray image is elongated along the laser beam axis. The emission region measures about 0.7 mm in height and consists of two parts. Its lower part is located opposite to the nozzle orifice (the emission peak is slightly higher than the nozzle axis) and corresponds to the radiation of the most dense paraxial jet region. The upper part is located significantly higher, upstream of the laser beam and corresponds to the emission of a more tenuous peripheral jet region. The absence of emission from the peripheral jet region downstream of the beam is quite explicable, because the plasma absorbs the greater part of the beam energy. According to calorimetric measurements, the beam energy transmitted through the gas target in different shots ranged from approximately 35 % to 5 % of the incident beam energy.

An absolute-calibrated AXUV-5 photodiode allowed us to measure the absolute X-ray yield in the reflection band of the focusing multilayer mirror (*4*) (Fig. 2) and also its dependence on the xenon pressure and the delay between the valve actuation and the laser shot. In this case it was noted that the lower the readings of the calorimeter (*8*), the higher the signal from the X-ray photodiode. For an above-nozzle xenon pressure of 8 bar and the optimal delay between the synchronising pulses, the electrical pulse recorded with the oscilloscope had a typical amplitude of 2 – 4 V for a half-maximum duration of ~ 18 ns (Fig. 5).

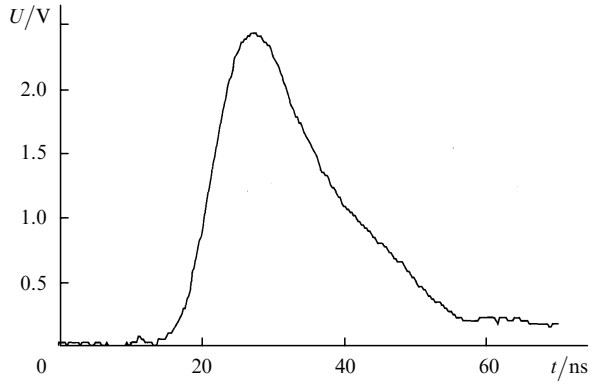

Figure 5. Typical electric pulse from the absolute-calibrated AXUV-5 photodiode.

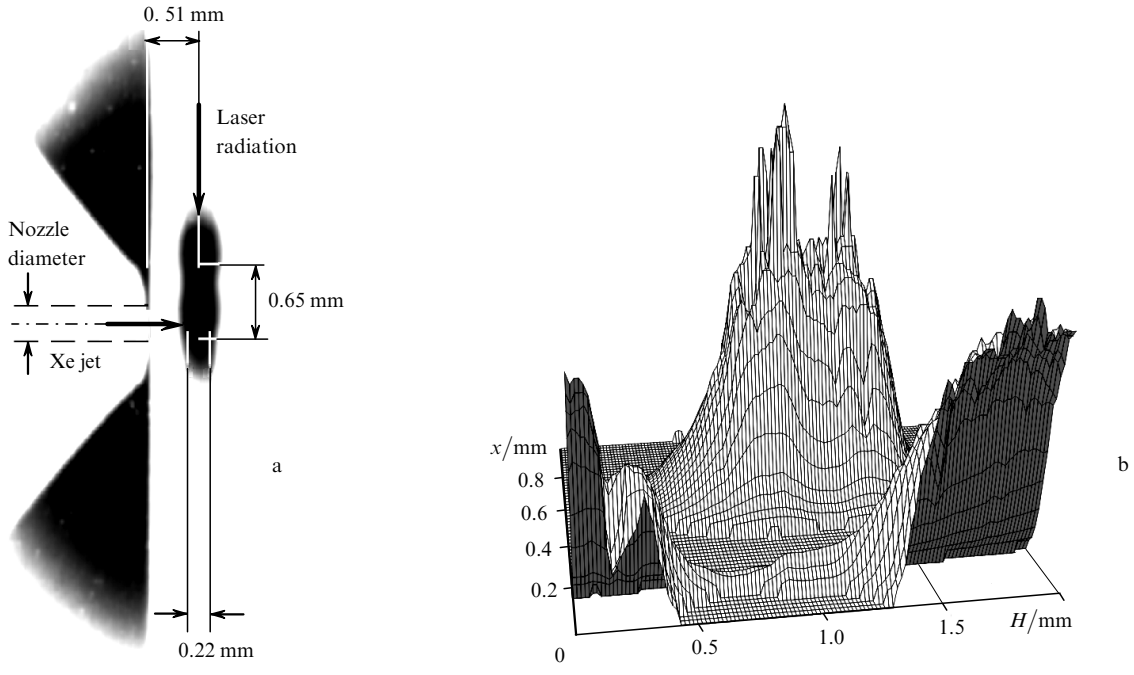

Figure 4. X-ray image of the xenon plasma in 175 – 185 Å wavelength band and the shadow of the nozzle cast in the visible light (a) and source intensity (b) (view 'from the nozzle', H is the vertical coordinate).

In the determination of the absolute yield, the main error could arise from the uncertainty of transmittance of the absorption filter. To reduce this uncertainty, we staged a dedicated experiment in which the filter was placed in the beam path in one of the diffraction orders of the broadband stigmatic spectrograph with a transmission grating with a density of 5000 lines mm^{-1}. A comparison of the exposures in the right and left (positive and negative) diffraction orders yielded an aluminium filter transmittance of ~ 0.20 at $\lambda = 180$ Å. The absolute spectral emittance of the source in the 180 Å range, determined with an AXUV-5 photodiode, was equal to 1.1×10^{-5} J sr^{-1} $Å^{-1}$, which corresponds to the laser radiation conversion efficiency of about 3×10^{-5} sr^{-1} $Å^{-1}$. The wavelength dependence of the emittance follows from the shape of the X-ray spectrum.

The xenon plasma emittance at $\lambda = 180$ Å was also determined independently in another way: from the optical density of the X-ray photographic film in the channel for recording the spectral image (Fig. 2). In this case, we relied on the absolute calibration of UF-4 X-ray photographic film performed in Ref. [13]. The xenon plasma emittance at $\lambda = 180$ Å thus determined was found to be equal to 9×10^{-6} J sr^{-1} $Å^{-1}$, which is in fairly good agreement with the data obtained with the AXUV-5 photodiode.

In the xenon spectrum in the 125–250 Å range we observed about a hundred spectral lines or unresolved line arrays most of which, to our knowledge, have not been classified. Fig. 6 shows a photograph of one of Xe spectrograms with indication of some identified lines belonging to Xe VIII–Xe X ions, and Fig. 7 shows the intensity distribution in this spectrum. The wavelengths of xenon ionic spectral lines ware borrowed from Refs [14, 15]. (For comparison we give the intensity distribution in the tungsten spectrum obtained by solid target irradiation.) Assuming the responsivity of the photographic film to be constant in the 125–250 Å range, we find that the integral emittance of both targets is approximately 1.1 mJ sr^{-1} in this range. In this case, the efficiency of laser radiation conversion to SXR that goes in a solid angle of 2π in the above spectral range is 2 %.

The emission peak in the Xe spectrum falls on the 145–170 Å range. The decrease in intensity for $\lambda < 145$ Å is supposedly due to the photoabsorption in the relatively cold periphery of the xenon jet which surrounds the plasma volume emitting in the SXR range (Fig. 4). This is confirmed by the fact that the fall in intensity in the short-wavelength part of the spectrum varies from experiment to experiment, which differ somewhat by the position of the laser beam axis relative to the jet axis, the absorbing layer thickness along line of sight changing in this case. The absorption can be so strong that the radiation with $\lambda \lesssim 150$ Å from the central segment of the plasma column is almost completely absorbed, and the emission from only the upper and lower segments can be observed.

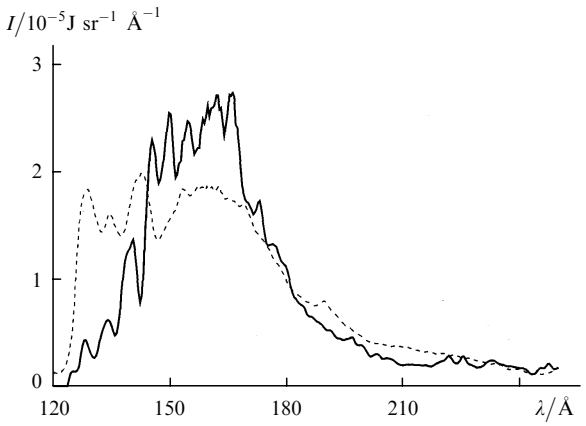

Figure 7. Intensity distributions I in the spectra of xenon (pulsed gas target, solid curve) and tungsten (solid target, dashed curve). In the case of a tungsten target, the direction of observation is close to the tangent to the surface of the flat target.

Fig. 8 shows a stigmatic spectrum in which the intensity in the short-wavelength portion was found to be strongly suppressed, especially so in the middle (in height H) segment of the plasma column. The observed 'splitting' in height (along the laser beam axis) is attributed to photoabsorption, which most strongly attenuates the emission from the central segment of the plasma column. This 'splitting' begins in the $\lambda \sim 160 - 170$ Å region and increases with decreasing wavelength. For $\lambda \sim 125$ Å it attains a value of about 1.3 mm – the full jet diameter at a distance of 0.5 mm from the nozzle. The grating has a regular support structure with a period of 4 μm perpendicular to the working lines. This produces, in addition to the main spectrum, lower-intensity spectra in the spectrogram which correspond to the $\pm$1st orders of diffraction by the support structure. These spectra are inclined by a small angle relative to the main one.

Fig. 9 shows the transmittance of a 0.5-mm thick layer of neutral xenon at a pressure of 0.08 bar (a density of

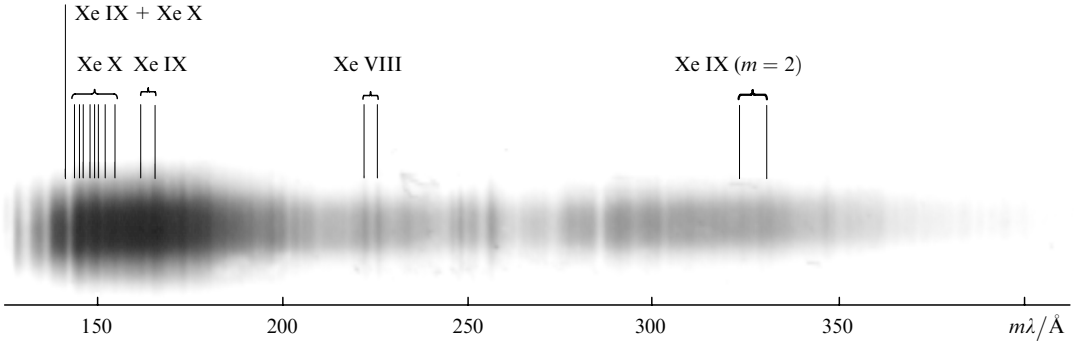

Figure 6. Xe spectrum with indication of several identified lines belonging to Xe VIII–Xe X ions, which was obtained with a 1000 line mm^{-1} transmission grating. The spectral resolution in the first order equal to 0.6 Å is determined by the slit width.

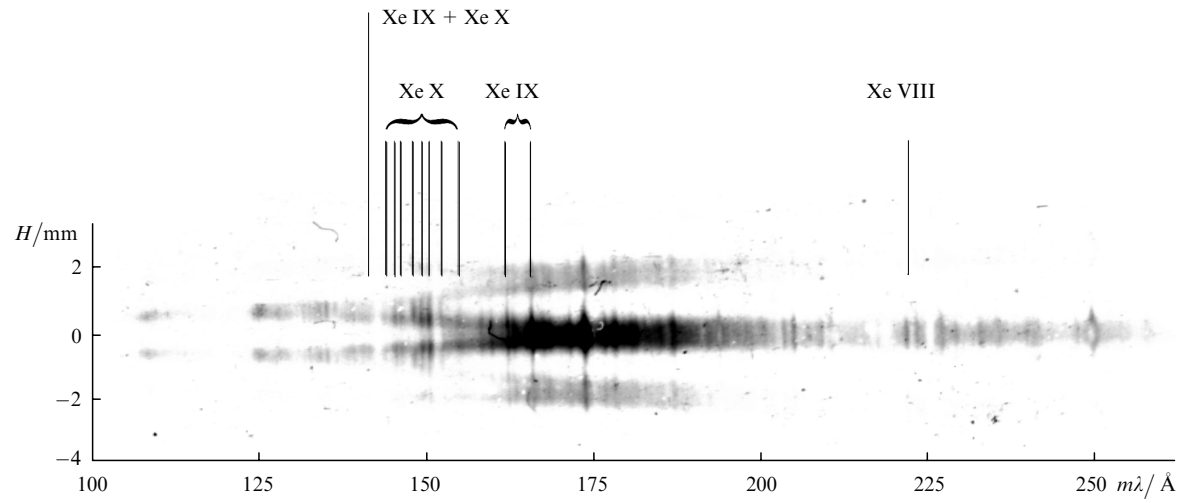

Figure 8. Photograph of a stigmatic Xe spectrum with indication of several lines belonging to Xe VIII – Xe X ions. Use was made of a 5000 line mm^{-1} grating.

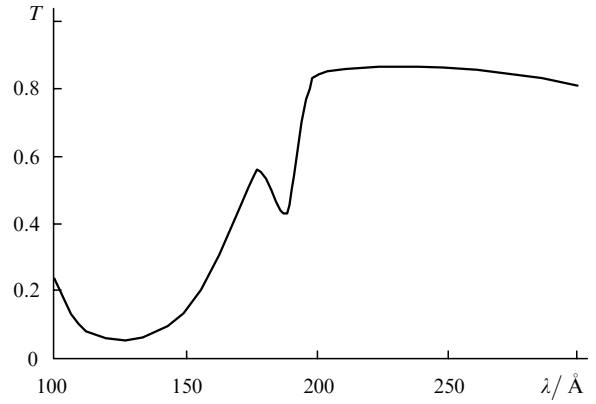

Figure 9. Transmittance T of a xenon layer with parameters characteristic for the jet at the point of laser beam focusing (the atomic xenon density is 2.2×10^{18} cm^{-3}, the layer thickness is 0.5 mm) calculated from the data of Ref. [16].

2.2×10^{18} cm^{-3}) calculated from the data of Ref. [16]. One can see that the absorption increases as the wavelength shortens from 200 to 125 Å, where the optical density $\tau = \mu_a N_{Xe\,I}\, r$ attains a value of three (μ_a is the photoabsorption cross section, N_{XeI} is the density of Xe I, and r is the jet radius). The strong photoabsorption in the wavelength range of interest is primarily related to the detachment of 4d electrons in neutral Xe I. (The 4d-electron binding energy in neutral Xe is equal to 69.5 eV, which corresponds to a wavelength of 178 Å.) Furthermore, low-charged xenon ions (Xe II, Xe II) produced in the photoionisation of the gas should also contribute to the absorption. The 4d-electron binding energy in ions increases as outer-shell electrons are removed (the outer electron shell of Xe I is $5s^2\,5p^6$).

In the long-wavelength region of the spectrum (Fig. 8) we observed a self-reversal of some spectral lines, which is supposedly due to the reabsorption in the nonuniform plasma.

Table 1. Xe VIII – Xe X ionic lines recorded in the spectrum of a pulsed xenon jet.

Ion	Transition	λ/Å	
Xe VIII	$5s^2S_{1/2} - 6p^2P_{3/2}$	221.841	
	$5s^2S_{1/2} - 6p^2P_{1/2}$	225.541	
Xe IX	$4d^{10}\,{}^1S_0 - 4d^9\,4f\,{}^3D_1$	143.618* }	143.65
	$4d^{10}\,{}^1S_0 - 4d^9\,5p\,{}^3D_1$	161.738	
	$4d^{10}\,{}^1S_0 - 4d^9\,5p\,{}^1P_1$	165.327	
		143.483** }	143.65
		145.153 }	145.04
		145.327 }	
		145.987 }	145.91
		146.152 }	
		147.624 }	147.75
		147.647	
		147.943	
		148.012 }	
Xe X	$4d^9 - 4d^8\,5p$	148.950 }	149.16
		149.028	
		149.366 }	
		150.095 }	150.26
		150.130	
		150.453	
		150.552 }	
		151.754 }	152.03
		151.762	
		152.065 }	
		154.442 }	154.58
		154.596	
		154.686 }	

*Blended with a Xe X line. **Blended with a Xe IX line.
Note. The braces are followed by the centres of gravity of the overlapping line groups.

4. Conclusions

A compact pulse-periodic laser-plasma debris-free SXR source was realised. The source was excited by the focused beam of a solid-state laser ($Q = 0.4$ J, $\tau_p = 6$ ns, $\lambda = 1.08$ μm) in a pulsed xenon jet. The source photographs were obtained and the source dimension was determined in

the radiation with a wavelength of 180 Å. The absolute radiation yield at this wavelength was 1.1×10^{-5} J sr^{-1} Å^{-1}. The energy distribution in the source spectrum in the 125–250 Å range peaks in the 145–170 Å interval. The short-wavelength portion of the spectrum is depressed due to the photoabsorption caused by the photoionisation of 4d electrons in neutral atoms and ions of xenon. It was possible to identify several lines belonging to Xe VIII–Xe X ions (see Table 1). The profiles of several ionic spectral lines are indicative of radiation reabsorption in the outer (cooler) plasma layers.

Acknowledgements. The authors are indebted to I.L.Beigman and P.V.Sasorov for helpful discussions; to N.V.Uvarova of NIIKhIMFOTOPROEKT Co. for providing excellent UF-4 X-ray photographic film; to F.Bijkerk of the FOM Institute for Plasma Physics Rijnhuizen, the Netherlands, for providing a large-aperture diffraction grating; and to V.A.Shatkov of the Neogaz Co. for his aid in istrumenting the experiment. The multilayer optical components were synthesised by V.V.Kondratenko and Yu.P.Pershin of the 'Kharkov Polytechnic Institute' National Technical University, Ukraine, whom we are grateful for long-term cooperation. This work was supported by the Russian Foundation for Basic Research (Grant No. 00-02-17717) and the 'Integration' Federal Dedicated Programme (Project No. AO133).

References

1. Fiedorowicz H., Bartnik ff., Kostecki J., Szczurek M., Fill E., Li Y., Lu P., Pretzler G., Nilsen J. *Proc. V Intern. Conf. on X-Ray Lasers* (Lund, Sweden, 1996) p. 76.
2. Filbert P.C., Kohler D.A., Walton R.A. *J. Appl. Phys.* **75**, 2332 (1994).
3. Altucci C., Bruzzese R., de Lisio C. et al. *J. Opt. A: Pure Appl. Opt.*, **2**, 289 (2000).
4. Paul P.M., Toma E.S., Breger P. et al. *Science*, **292**, 1689 (2001).
5. De Bruijn R., Bartnik A., Fledderus H.F., Fiedorowicz H., Hegeman P., Constantinescu R.C., Bijkerk F. *Proc. SPIE Int. Soc. Opt. Eng.,* **3997**, 157 (2000).
6. Gullikson E.M., Underwood J.H., Batson P.C., Nikitin V. *J. X-Ray Sci. Technol.*, **3**, 283 (1992).
7. Zhitnik I.A., Kuzin S.V., Mitropol'skii M.M., Ragozin E.N., Slemzin V.A., Sukhanovskii V.A. *Kvantovaya Elektron.*, **20**, 89 (1993) [*Quantum Electron.,* **23**, 76 (1993)].
8. Ragozin E.N., Kolachevsky N.N., Mitropolsky M.M., Pokrovsky Yu.Yu. *Proc. SPIE Int. Soc. Opt. Eng.*, **3113**, 230 (1997).
9. Kondratenko V.V., Levashov V.E., Pershin Yu.P., Pirozhkov A.S., Ragozin E.N. *Kr. Soobshch. Fiz. FIAN* (7), 32 (2001).
10. Kolachevskii N.N., Pirozhkov A.S., Ragozin E.N. *Kr. Soobshch. Fiz. FIAN* (12), 55 (1998).
11. Kolachevskii N.N., Pirozhkov A.S., Ragozin E.N. *Kvantovaya Elektron.*, **30**, 428 (2000) [*Quantum Electron.*, **30**, 428 (2000)].
12. Beigman I.L., Pirozhkov A.S., Ragozin E.N. *Pis'ma Zh. Eksp. Teor. Fiz.*, **74**, 149 (2001) [*Exper. Theor. Phys. Lett.*, **74**, 149 (2001)].
13. Shevel'ko A.P. *Kvantovaya Elektron.*, **23**, 748 (1996) [*Quantum Electron.*, **26**, 729 (1996)].
14. Kaufman V., Sugar J. *Phys. Scr.*, **24**, 738 (1981).
15. Kaufman V., Sugar J., Tech J.L. *J. Opt. Soc. Am.*, **73**, 691 (1983).
16. Soufli R., Gullikson E.M. *Proc. SPIE Int. Soc. Opt. Eng.,* **3113**, 222 (1997); http://cindy.lbl.gov/optical_constants/.